Integer ambiguity resolution on undifferenced GPS phase measurements and its application to PPP and satellite precise orbit determination

D. Laurichesse, F. Mercier, J.P. Berthias, P. Broca, L. Cerri
C.N.E.S, France

ABSTRACT

Integer ambiguity fixing is routinely applied to double-differenced GPS phase measurements to achieve precise positioning. Double-differencing is interesting because it removes most of the common errors between the different signal paths. However, if common errors can be estimated it becomes attractive to fix integer ambiguities on undifferenced measurements: phase measurements then become pseudorange-like measurements with a noise level of a few millimeters.

This paper introduces a new method for fixing dual-frequency GPS ambiguities on undifferenced phase measurements either locally or globally. The clocks for the GPS constellation obtained during this process can be used for precise point positioning of ground based receivers and for precise orbit determination of low Earth orbiting satellites. The resulting positioning precision is comparable to that of standard differential positioning without the need for a reference station. Ambiguity-fixed satellite orbits for the GRACE and Jason satellites are more precise than the most precise solution available today.

INTRODUCTION

The fixing of phase integer ambiguities is a key element of precise GPS applications [1]. Usually, integer constraints are only applied to phase double differences, because all unknown non-integer common biases are eliminated by the differentiation process. An alternate approach is to work on simple differences, either station-station differences [2], or satellite-satellite differences [3], with interesting results.

An even more challenging problem is to work directly on undifferenced measurements [4, 5, 6]. A new method for fixing undifferenced integer phase ambiguities is presented in the first half of this paper, followed by applications to precise point positioning of ground-based receivers and to the precise orbit determination of Low Earth orbit satellites. This method involves two independent steps: first undifferenced widelane ambiguities are estimated for each receiver following the identification of biases for the GPS constellation, then L_1 ambiguities are fixed over a network. The starting geometry and troposphere delays are given by a standard floating solution of the problem. The complete process fixes about 90% of all elementary ambiguities over the entire network.

MODEL EQUATIONS

In this paper, we use the following notations:

$$\gamma = \frac{f_1^2}{f_2^2}, \quad \lambda_1 = \frac{c}{f_1}, \quad \lambda_2 = \frac{c}{f_2}$$

where f_1 and f_2 are the two frequencies of the GPS system and c is the speed of light. For GPS L_1 and L_2 bands, $f_1 = 154 f_0$ and $f_2 = 120 f_0$, where $f_0 = 10.23\,\mathbf{MHz}$. Pseudorange or code measurements, P_1 and P_2, are expressed in meters, while phase measurements, L_1 and L_2, are expressed in cycles.

The pseudorange and phase measurements are modeled as:

$$\begin{array}{lccccc} P_1 = & D_1 & +e & +\Delta h_p & +\Delta\tau_p & \\ P_2 = & D_2 & +\gamma e & +\Delta h_p & +\gamma\Delta\tau_p & \\ \lambda_1 L_1 = & D_1 + \lambda_1 W & -e & +\Delta h & +\Delta\tau & -\lambda_1 N_1 \\ \lambda_2 L_2 = & D_2 + \lambda_2 W & -\gamma e & +\Delta h & +\gamma\Delta\tau & -\lambda_2 N_2 \end{array} \qquad (1)$$

where:

- D_1 and D_2 are the geometrical propagation distances between the emitter and receiver phase centers at f_1 and f_2 including troposphere elongation, relativistic effects, etc.
- W is the contribution of the wind-up effect (in cycles).
- e is the ionosphere elongation in meters at f_1. This elongation varies with the inverse of the square of the frequency and with opposite signs between phase and code.
- $\Delta h = h_i - h^j$ is the difference between receiver i and emitter j ionosphere-free phase clocks. Δh_p is the corresponding term for pseudo-range clocks.
- $\Delta\tau = \tau_i - \tau^j$ is the difference between receiver i and emitter j offsets between the phase clocks at f_1 and the ionosphere-free phase clocks. By construction, the corresponding quantity at f_2 is $\gamma\Delta\tau$. Similarly, the corresponding quantity for pseudorange is $\Delta\tau_p$ (Time Group Delay).
- N_1 and N_2 are the two carrier phase ambiguities. By definition, these ambiguities are integers. Unambiguous phases measurements are therefore $L_1 + N_1$ and $L_2 + N_2$.

These equations take into account all the biases related to delays and clocks. The four independent parameters $\Delta h, \Delta\tau, \Delta h_p, \Delta\tau_p$ are equivalent to the definition of one clock per observable. However, this choice of parameters

emphasizes the specific nature of the problem by identifying reference clocks for pseudorange and phase (Δh_p and Δh) and the corresponding hardware offsets ($\Delta \tau_p$ and $\Delta \tau$). These offsets are assumed to have slow variations with time, with limited amplitudes. The offset between phase and pseudorange clocks $\Delta h - \Delta h_p$ has similar slow limited variations, as shown by direct comparison of code and phase residuals [7].

Additionally, we define the widelane ambiguity $N_w = N_2 - N_1$. This quantity is an integer, with an associated wavelength λ_w given by $\frac{1}{\lambda_w} = \frac{1}{\lambda_1} - \frac{1}{\lambda_2}$ (around 87 cm for GPS L_1 and L_2 bands).

We define the measured pseudorange ionosphere elongation and the measured ambiguities by

$$e_P = \frac{P_1 - P_2}{1-\gamma} \qquad \tilde{N}_1 = \frac{P_1 - 2e_P}{\lambda_1} - L_1 \qquad \tilde{N}_2 = \frac{P_2 - 2\gamma e_P}{\lambda_2} - L_2 \qquad (2)$$

These three quantities depend only on measurements. The noise level of pseudorange measurements is too large to estimate ambiguities at the cycle level using $\tilde{N}_1$ and $\tilde{N}_2$ with a single pass of data. Indeed, the typical noise on these quantities is about 10 cycles. This is why we focus first on the widelane ambiguity whose wavelength is larger.

We note $\tilde{N}_w$ the measured widelane $\tilde{N}_w = \tilde{N}_2 - \tilde{N}_1$ (also called the Melbourne-Wübbena widelane). Substituting (1) in (2), it is possible to express $\tilde{N}_w$ as

$$\tilde{N}_w = N_w + d + \left(\mu_i - \mu^j\right) \qquad (3)$$

where μ_i is a linear combination of τ_i, $\tau_{p,i}$ and $h_i - h_{p,i}$ and μ^j is a linear combination of τ^j, ${\tau_p}^j$ and $h^j - {h_p}^j$. $d = 2(D_1 - D_2)/(\lambda_1 + \lambda_2)$ is non-zero because of the offset between the phase center locations at L_1 and L_2. Its value is generally below 0.1 widelane cycles with current geodetic antennas where the two phase centers are only a few centimeters apart. The fluctuations in (3) over a pass are thus generally well below one cycle.

By averaging (3) over the duration of a pass:

$$\left\langle \tilde{N}_w \right\rangle \approx N_w + \left\langle \mu_i \right\rangle - \left\langle \mu^j \right\rangle \qquad (4)$$

where the contribution of $\langle d \rangle$ is neglected. The noise on $\left\langle \tilde{N}_w \right\rangle$ is usually small enough to lead to a correct estimate of the integer N_w and, as a consequence, of μ_i and μ^j. It can be shown that the widelane delays for GPS satellites μ^j are constant over long periods of time [8]. Note that there is an infinity of solutions to equations (3), since it is

possible to shift N_w by any integer number of cycles, modifying the μ 's accordingly. This is the reason why only the fractional parts of the μ 's are observable. Also, without any other constraint, the problem remains singular, because the equations only contain the differences $\mu_i - \mu^j$; μ_i and μ^j are thus each defined up to an unknown floating constant.

FRACTIONAL WIDELANE DELAYS IDENTIFICATION PROCESS

The fractional widelane delays are estimated for a network of stations and the whole GPS constellation. In this section, we assume that fractional widelane delays have limited variations over the duration of the processed data set (typically around 0.1 cycle). This is usually true for geodetic receivers in good operating conditions (for example IGS receivers) [8].

The set of all equations (4) for all passes over the network can be rewritten in the following form

$$R_i^j = \mu_i - \mu^j \quad \text{for receiver } i \text{ and emitter } j$$

There are as many equations as passes, with R_i^j equals to the mean widelane estimate of the pass modulo 1. However, to ensure consistency between all the passes of a given station-satellite pair, some of the R_i^j values are shifted by +1 or -1 to keep them all close to each other. Outliers between different passes on the same station-satellite pair are eliminated during this process.

At this stage, some inconsistencies might remain in the integer part of the R_i^j s, for example for different stations listening to the same satellite. In order to correct this problem, a reference station i_0 is chosen and a first estimate of all satellite μ^j s is constructed ${}_1\mu^j = -R_{i_0}^j$. This estimate is then used to compute all station biases ${}_1\mu_i = {}_1R_i^j + {}_1\mu^j$. These equalities are generally not directly compatible because small integer inconsistencies remain in the choice of ${}_1R_i^j$. After correction of these inconsistencies and elimination of the outliers, the ${}_1\mu_i$ s are estimated in the least square sense. The values of ${}_1\mu_i$ and ${}_1\mu^j$ are then substituted in all the equations and the corresponding integer corrections on the R_i^j s are fixed once and for all. Then new estimates for ${}_2\mu_i$ and ${}_2\mu^j$ are computed using a standard batch least squares for all passes. The final residuals on all equations are below a fraction of cycle (typically 0.2 cycles).

EXPERIMENTAL RESULTS ON THE FRACTIONAL WIDELANE DELAYS

Figure 1 shows raw measured widelanes computed from undifferenced code and phase measurements from a given station (upper plot), and the same quantities corrected with the μ^j (lower plot). The aggregation of corrected measured widelanes around integers is clearly visible on the lower plot. It is then easy to identify the associated integer widelanes N_w since the noise is far below one widelane cycle. The receiver widelane delay μ_i can then be determined as a by-product.

We have processed data from a large selection of IGS receivers and we have found that the same values for the satellite widelane delays μ^j can be used for all the semi-codeless receivers that we have tested. Codeless receivers based on different technologies, such as Trimble™ receivers, lead to a different set of satellite widelane delays μ^j due to the use of other pseudo-ranges references. The relationship between satellite widelane delays for different families of receivers can be computed by processing data from nearby receivers [8].

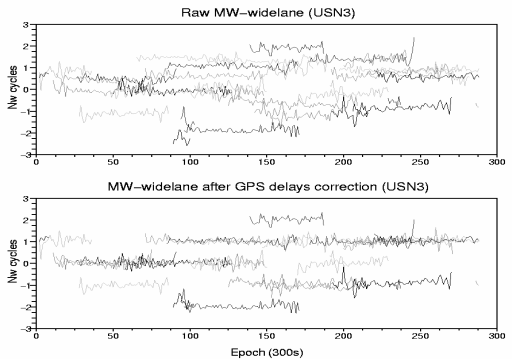

Fig. 1. Floating versus Integer N_w residuals (USN3)

Figure 2 shows the widelane ambiguity residuals, corrected by μ^j, after removal of the identified integer values.

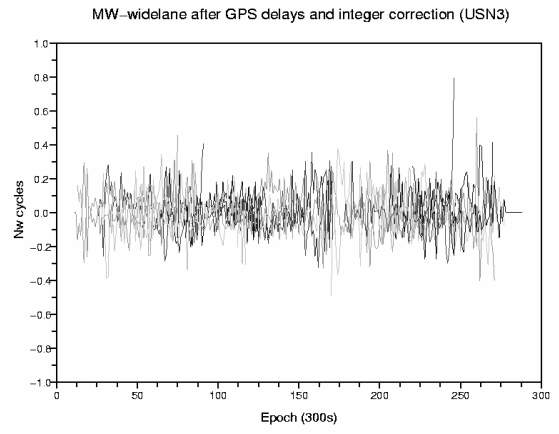

Fig. 2. N_w residuals after corrections (USN3)

BENEFITS OF UNDIFFERENCED WIDELANE COMPUTATION

Once satellite widelane delays are known, it is possible to fix widelane ambiguities at the undifferenced measurement level for all receivers, without having to compute differences with any other receiver. This characteristic is particularly useful for isolated receivers such as hand-held moving devices which have no access to any reference station. In addition, the fact that μ^j's are unique and identical guarantees that the ambiguity fixing will be coherent over the entire network.

N_1 IDENTIFICATION

After widelane fixing, only one ambiguity, N_1 or N_2, or any combination of N_1 and N_2, is left unknown. The ionosphere free combination is the best candidate as it eliminates the contribution from the ionosphere.

$$P_c = \frac{\gamma P_1 - P_2}{\gamma - 1}$$
$$\hat{Q}_c = \frac{\gamma\lambda_1\left(L_1 + \hat{N}_1\right) - \lambda_2\left(L_2 + \hat{N}_1 + N_w\right)}{\gamma - 1} \qquad (5)$$

where $\hat{N}_1$ is the best estimate of N_1 that is the closest integer to $\left\langle \tilde{N}_1 \right\rangle$,

$$\left\langle \tilde{N}_1 \right\rangle = \left\langle \frac{P_1 - 2e_P}{\lambda_1} - L_1 \right\rangle .$$

The noise level on the pseudorange data is such that the difference between $\hat{N}_1$ and the true value of N_1 can be as high as 10 cycles.

Pc is the ionosphere-free code combination. $\hat{Q}_c$ is the best approximation of the ionosphere-free unambiguous phase combination

$$Q_c = \frac{\gamma\lambda_1(L_1 + N_1) - \lambda_2(L_2 + N_1 + N_w)}{\gamma - 1}$$

Given the fact that N_W is known, the problem of finding the ionosphere-free ambiguity is replaced by the problem of finding N_1

$$Q_c = \frac{\gamma\lambda_1 L_1 - \lambda_2 L_2}{\gamma - 1} - \frac{\lambda_2}{\gamma - 1} N_W + \lambda_c N_1$$

with $\lambda_c = (\gamma\lambda_1 - \lambda_2)/(\gamma - 1) \approx 10.6\,\text{cm}$. In practice, rather than solving for N_1 we solve for the ambiguity correction $\delta N_1 = \hat{N}_1 - N_1$. Substituting (1) in (5) leads to

$$\begin{aligned} P_c &= D + \Delta h_p \\ \hat{Q}_c &= D_w + \Delta h + \lambda_c \delta N_1 \end{aligned}$$

where D is the geometrical distance between ionosphere free phase centers $D = (D_2 - \gamma D_1)/(1 - \gamma)$ and $D_w = D + \lambda_c W$ also takes into account the windup contribution.

In order to estimate δN_1 we first need precise estimates for the propagation distance D_w and for the clocks. These are obtained by standard positioning using a network of receivers. This positioning is performed with a filter which processes pseudorange P_c and phase $\hat{Q}_c$ (with respective noises of 1m and 1cm), and solves for emitter and receiver clocks at each epoch, floating δN_1 ambiguities per pass and zenith troposphere delays constant per two hour period (zenith delays are mapped to all elevations using the Stanag function). Typically, using state-of-the art correction models (satellite attitude, station displacements, etc.) residual errors are at the centimeter level.

Once D_w and clocks are known the ambiguity correction can be computed from

$$\delta N_1 = (\hat{Q}_c - D_w - \Delta h) / \lambda_c$$

The resulting values are not integers because no integer constraint was applied during the previous filtering. The fluctuations in the estimated clocks hide the integers. Integers are revealed when computing station-station simple differences and thus removing h^j's (cf. Figure 3).

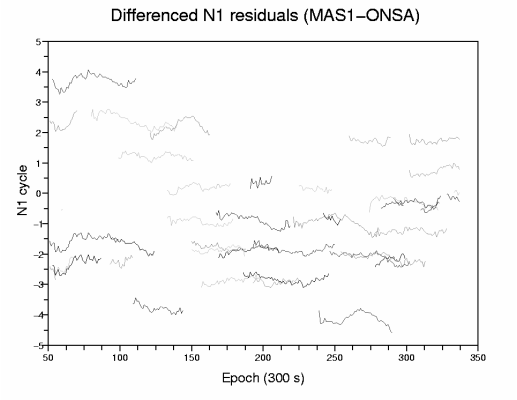

Fig. 3. Long baseline N_1 single differences

The global variations in Figure 3 are due to fluctuations of h_i 's. The differences between each of the curves are integers. After identification and removal of these integers, residuals fall below 0.2 cycles (cf. Figure 4).

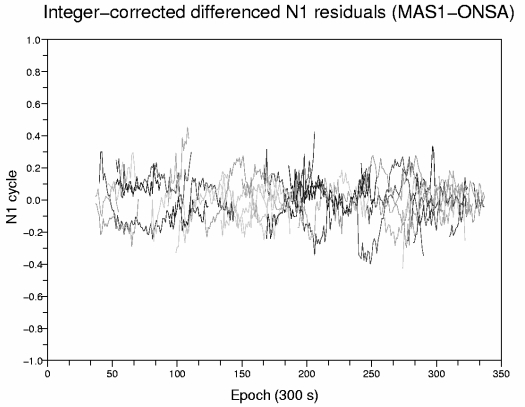

Fig. 4. N_1 Residuals after corrections

Experimentally it was found that this method identifies integer values for baselines up to 3000 km.

The integer problem can be reformulated as follows

$$\hat{Q}_c - D_w = \lambda_c \delta N_1 + h_i - h^j \qquad (6)$$

in order to solve for one integer value for δN_1 per pass and one set of clocks per epoch (no assumption is made on the continuity of clocks over time).

Equations (6) have the same structure as equations (4), where delays have been replaced by clocks. The key difference is that clocks have to be identified at each epoch. Observability problems are the same as for equations (4). The solution is the following. First a reference station is chosen and δN_1 and h_i are set to zero for this station.

Then h^j 's for all the satellites in view of this station are computed using equation (6). Then we add a new station as follows: with the set of current h^j, we compute the quantities $\delta N_1 + h_i / \lambda_c$ using (6). We have to express this quantity with one integer value per pass (δN_1), and one floating value per epoch (h_i / λ_c). As seen on Figure 3, this separation can be done easily. We note that, for a new station, the satellite clocks are known only for a fraction of the passes (since we use a differencing process), but, as δN_1 is constant per pass, we can extend it to the totality of the pass. To maximize the chance of finding new valid ambiguities, it is pertinent to choose a new station close to the previous ones. Once all the stations have been included, we identify a set of integer values for all δN_1. As a by-product, we obtain the corresponding set of h^j. This process can be applied to a local area (a zone like the United States of America or Europe), or to the entire globe. The h_i and h^j clocks are called 'integer' clocks hereafter, to emphasize the specific properties of equation (6) [8].

OVERVIEW OF THE COMPLETE FIXING PROCESS

Figure 5 depicts the entire fixing process. The input is a set of raw RINEX files (one per station, typically for 100 stations). First, all the widelanes are fixed on an independent basis. Then, D is computed by filtering. Finally, the process described in the previous section is used to fix the remaining ambiguities. The main product of the process is a set of RINEX files (one per station) in which all the phase ambiguities are fixed. These measurements can then be processed by a standard orbit determination and time synchronization software, except that there is no need to estimate floating ambiguities anymore. This results in a significant improvement in the observability of the estimated parameters, which can include GPS orbits and clocks, zenith troposphere delays, stations coordinates and clocks, polar motion, length of day, phase maps, etc. The analysis of all of these improvements is beyond the scope of this paper.

One of the main advantages of the undifferenced solution over the station-station simple difference solution is that GPS clocks are estimated. In the remainder of this paper, we focus on the use of these clocks for positioning of user receivers.

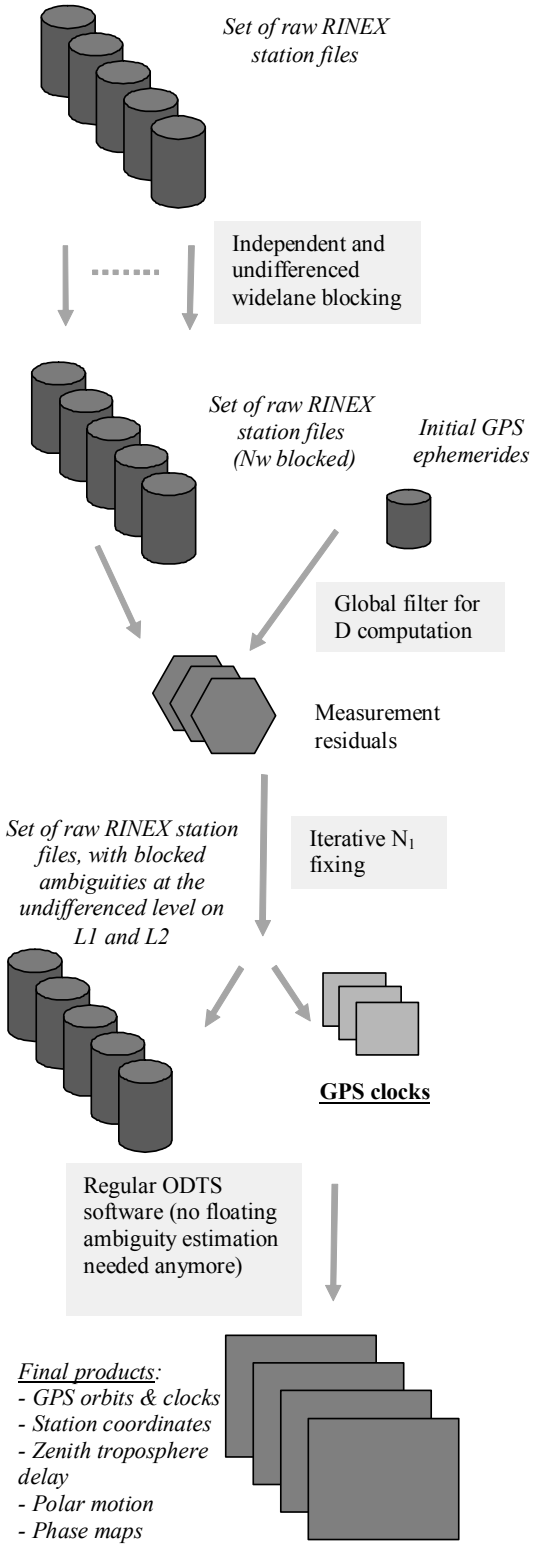

Fig. 5. Flow diagram of ambiguity resolution process

APPLICATION TO POINT POSITIONING

PPP EXPERIMENTAL SET-UP

For our experiment, we have chosen the following set-up (Figure 6):

- A local network of 10 IGS stations located in Western Europe. These stations are used to compute the GPS clocks.

- Another IGS station (TLSE), which is not part of the previous network. This station, located on the CNES Toulouse campus, is used to investigate the properties of the integer GPS clocks, and serves as a reference station for relative positioning of proximity receivers.

- A hand-held moving receiver (Septentrio PolarX2), also located on the CNES campus (within a few hundred meters of the TLSE station).

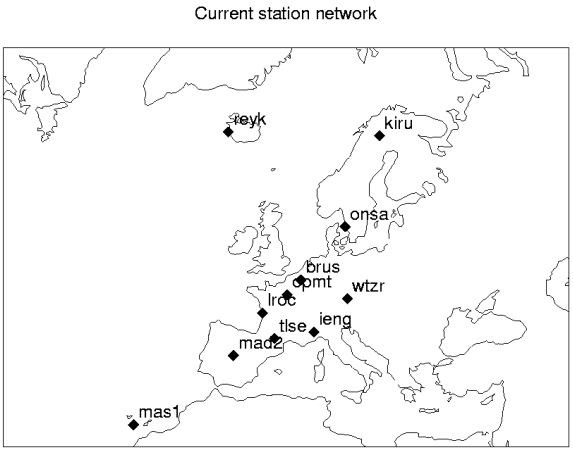

Fig. 6. Station network

The test date is July 2, 2007. All the IGS stations use the same values for μ^j's because the receivers are all semi-codeless. The Trimble™ receiver of the TLSE station requires the use of different values because of differences in technology (cross-correlated receiver) [8]. Table 1 gives the values of the μ^j's for that day.

Table 1. Emitter widelane delays for 2 July 2007

(unit widelane cycles)

PRN	semi codeless	cross correlated	PRN	semi codeless	cross correlated	PRN	semi codeless	cross correlated	PRN	semi codeless	cross correlated
1	**0.46**	**0.39**	**9**	**0.36**	**0.07**	**17**	**-0.30**	**-1.05**	**25**	**-0.20**	**-0.60**
2	**-0.20**	**-0.49**	**10**	**-0.60**	**-0.18**	**18**	**-0.40**	**-0.44**	**26**	**-0.28**	**-0.92**
3	**-0.74**	**-0.68**	**11**	**-0.29**	**-0.76**	**19**	**-0.10**	**0.31**	**27**	**0.20**	**0.17**
4	**-0.21**	**-0.95**	**12**	**-0.10**	**-0.82**	**20**	**0.10**	**0.34**	**28**	**0.49**	**0.30**

5	**0.10**	**0.29**	**13**	**0.31**	**-0.48**	**21**	**0.50**	**0.33**	**29**	**-0.26**	**-0.64**
6	**0.40**	**-0.01**	**14**	**0.01**	**-0.20**	**22**	**-0.43**	**-0.88**	**30**	**0.40**	**-0.50**
7	**-0.48**	**-0.40**	**15**	**0.00**	**0.32**	**23**	**0.25**	**-0.40**	**31**	**0.13**	**-0.73**
8	**0.31**	**0.09**	**16**	**-0.05**	**-0.07**	**24**	**0.13**	**-0.03**	**32**	**0.44**	**0.00**

Daily GPS data files and precise ephemerides are obtained from the IGS [9]. After widelane fixing, GPS and station clocks, as well as troposphere zenith propagation delays, are computed using the standard positioning process described above. While μ^j's can be considered as constants, μ_i's, which are equivalent to integer narrowlane clocks, are not constant and must be identified at each epoch.

Table 2 shows the fixing success rate for N_1 passes. This success rate is the ratio between the number of fixed ambiguities and the total number of ambiguities which were not eliminated during the widelane identification process.

Table 2. N_1 fixing success rate

Station	Success rate (%)	RMS (mm)
lroc	91.3	7.2
mad2	93.1	9.6
brus	100.0	8.8
onsa	93.5	8.8
mas1	100.0	9.1
ieng	97.7	8.1
wtzr	91.1	9.1
reyk	76.9	11.3
nico	78.9	14.4
kiru	62.7	10.4
mean	**88.5**	**9.7**

'COMPACT' REPRESENTATION

The N_1 residuals for the TLSE receiver, which is not included in the network solution, are a good test of the quality of the integer clocks.

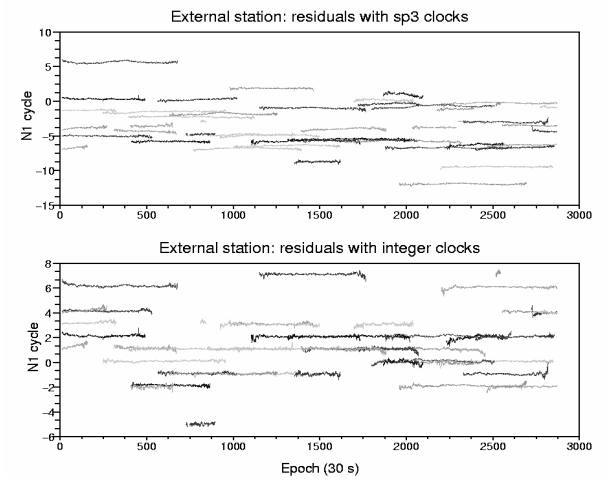

Fig. 7. Floating versus Integer N_1 residuals

The upper plot of Figure 7 shows the N_1 residuals for TLSE computed using IGS clocks, the lower plot shows the same quantity computed using integer clocks: the integer cycle aggregation of residuals is clearly enhanced by integer clocks. This shows that the ambiguity fixing information of the network can be concentrated in the GPS satellite clocks: an external receiver which has access to integer clocks can easily estimate its own N_1 ambiguities without any additional external data.

We have thus transformed the observation representation data into a compact representation [10] where the only elements needed for worldwide absolute precise positioning are the widelane delays μ^j's for the GPS satellites (and for each family of receivers - we have identified only four families), and the GPS satellite positions and integer clocks at each epoch. These parameters are sufficient for any receiver anywhere in the world to fix its ambiguities in an independent manner.

The broadcasting of this compact representation would require a relatively low bandwidth. It would provide an easy way to perform Integer-PPP anywhere without any reference station.

POSITIONING RESULTS FOR A GEODETIC RECEIVER

We have tested the self-fixing process described above on the TLSE station. The input data (one day, 30 s sampling) were given in the compact representation. All the ambiguities were then fixed.

We ran a first positioning test using a Kalman filter. The estimated parameters were the position (3-D), a stochastic clock and a slowly varying zenith troposphere delay. The model noise was set to a small value to smooth the

positioning result. Figure 8 shows the positioning error in the horizontal plane. The error is within a 2 by 2 cm square.

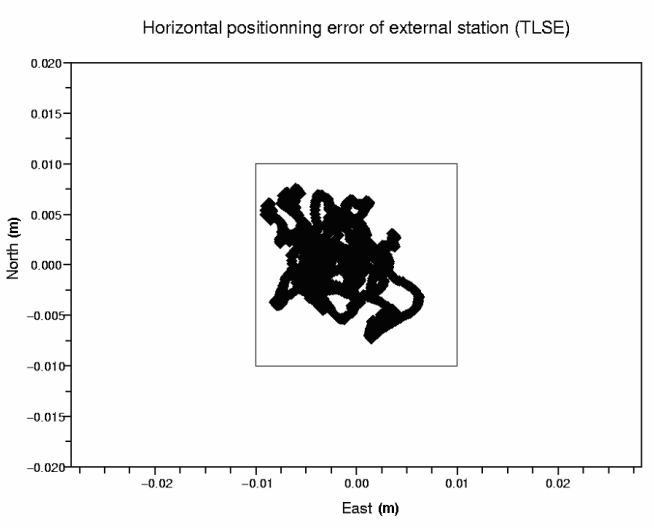

Fig. 8. Static geodetic receiver positioning error

In a second run we have suppressed the station displacement correction due to solid-Earth tides in the modeling of the distance, thus creating a virtual diurnal motion whose largest component is about 20 cm on the vertical. The model noise for the position was tuned accordingly.

On Figure 9, the smooth curves represent, in a local geographical reference frame, the reference model for the tidal displacement, and the noisy ones the position estimated by the filter. These curves agree at the 1 cm level RMS.

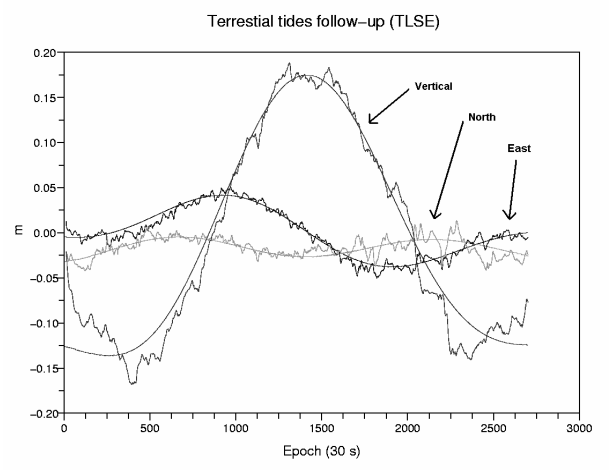

Fig. 9. Virtual slowly moving geodetic receiver

POSITIONING RESULTS FOR A MOVING HAND-HELD RECEIVER

Another experiment was conducted with the hand-held Septentrio PolarX2 receiver with a patch antenna. In such experiments, one problem is having a good knowledge of the reference trajectory. The experiment took place on the CNES campus in Toulouse, France. The setup consisted of an arm on top on a tripod, with the antenna fixed at the far end of the arm, in order to describe a circle of around 80 cm in diameter.

The experiment was performed in two phases:

- A static phase: 1 hour of measurements with the antenna fixed.
- A moving phase: 1 hour of measurements with the antenna moving around the circle (one rotation).

The interest of the static phase is twofold: first to assess the quality of integer positioning in static mode, and second to allow the fixing of ambiguities as initial conditions for the moving phase. This static phase is not mandatory, but experience shows that it shortens significantly the time required for ambiguity fixing. This is due to the fact that only one constant position has to be estimated during the entire static phase. When the receiver is moving during the initialization phase, its position must be estimated at each epoch, and ambiguities are less observable. The tests that we have conducted show that the initial ambiguities can be fixed with a good confidence level in about 30 minutes when the receiver is not moving, whereas it takes around 90 minutes to fix ambiguities when the receiver is moving.

Figure 10 shows the PRN number of the satellites in view during the experiment, during both phases. It is interesting to note that although we have seven satellites in view almost all the time, a few of them have changed between the two phases. This was not done on purpose.

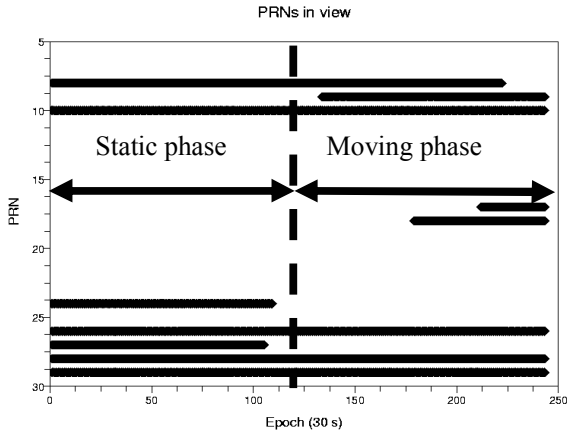

Fig. 10. Satellites in view

The autonomous widelane fixing performance was verified by processing simple differences with the LROC station. As shown on Figure 11 the widelane delay on the receiver's side ($\widetilde{N}_w - N_w + \mu^j$) is far from constant. The envelope represents the mean of the residuals plus and minus one cycle. For this kind of receiver, the assumption of a constant delay over one day, like for receivers in geodetic conditions, is clearly not valid. The reason for these variations is unknown; it might be because the receiver was running on its internal oscillator (the receiver suffered several millisecond jumps during the 2 hours of the experiment) and also because the receiver was turned on just before the experiment (thermals effects).

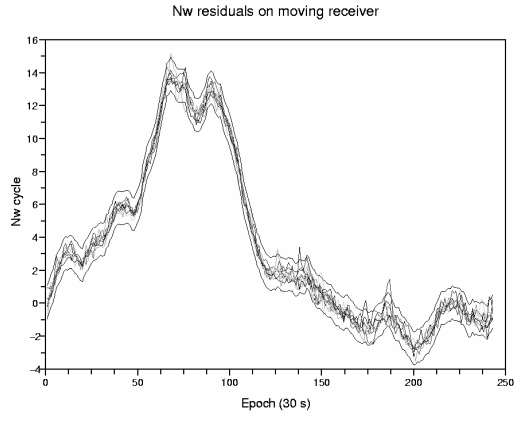

Fig. 11. Receiver widelane delay evolution

After widelane ambiguity fixing, GPS integer clocks were used to estimate the N_1 ambiguities on the receiver side. First the static phase was processed as follows:

- A standard least squares filtering adjusted the stochastic receiver clock, one constant 3-D position, one constant zenith troposphere delay and one floating ambiguity per pass,
- Then the integer domain was searched for the nearest position that would fix all N_1 ambiguities with residuals less than 0.2 cycles (only one solution was found in a 3 cm cube around the initial floating position),
- A last least squares filtering with ambiguities set to their integer values provided the receiver position and clock and the troposphere delay which served as initial conditions for the moving phase.

Then the moving phase was processed:

- A standard least squares filtering adjusted the stochastic receiver clock, the stochastic 3-D receiver position, one constant zenith troposphere delay and one floating ambiguity per pass for passes whose ambiguities were not fixed during the static phase,

- Then the new floating ambiguities were fixed (they are so close to integers that they can simply be rounded off to the nearest integer),
- A last least squares filtering with ambiguities set to their integer values provided the receiver trajectory.

This final trajectory is the location of the ionosphere-free phase center of the receiver's antenna.

The reference trajectory was computed using single differences with the TLSE station, located at a distance of about 100 m. L_1 and L_2 phase measurements were processed separately, and ambiguities fixed independently on each frequency. Then a precise reference trajectory was computed for the L_1, L_2 and then L_c (ionosphere-free) phase centers.

Figure 12 shows the various trajectories projected onto the horizontal plane: the L_1 and L_c references and the L_c trajectory estimated by our method. The zoom in the middle of Figure 12 shows the results of the static phase: the three solutions are within a 1 by 1 cm square.

The L_1 reference trajectory appears to be closer to the physical circle described by the antenna than the other solutions: this is due to the very good quality of L_1 measurements. The L_c reference is noisier because of the noise on L_2, which is amplified by the ionosphere-free combination. The noise on the L_c trajectory computed using our method is similar to that of the L_c reference. The RMS of the difference between any two solutions is around 1 cm.

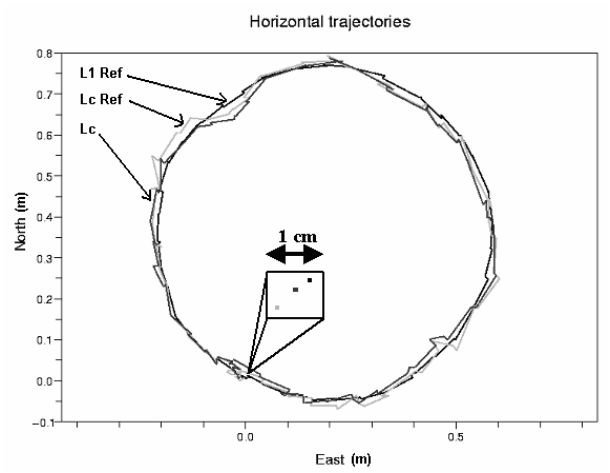

Fig. 12. Receiver reconstructed trajectories

EXTENSION TO REAL-TIME

The previous experiment was conducted by recording data and processing them afterwards. However it is also possible to extend our approach to real-time processing [11]. In this case widelane ambiguities at the receiver level can usually be fixed after 5 to 30 minutes, mainly depending on the elevation angle of measurements. The

parameters of the 'compact' representation can then be computed in real-time, using a modified Kalman filter. The robustness of this method was evaluated using the EUREF-IP (EUropean REference Frame - Internet Protocol) GNSS data stream [11]. From the ground user point of view, the initialization time (i.e. the time to start fixing the receiver ambiguities to their integer values) is not increased with respect to standard PPP: the observability comes from the slowly moving geometry of the GPS satellites so an initialization time from 30 minutes to one hour is standard. The real-time user positioning precision is 1 cm RMS, equivalent to the one obtained in post-processing.

APPLICATION TO SATELLITE PRECISE ORBIT DETERMINATION

The method can be extended to the precise orbit determination of Low Earth Orbit (LEO) satellites provided that the spaceborne GPS receivers carried on-board are compatible with the widelane fixing technique. For N_1 fixing, added difficulties are the high dynamics of the satellite and the short passes (around 15 minutes). Once widelane and N_1 fixing are performed, any standard orbit determination filter can take advantage of the increased observability provided by unambiguous phase data to improve orbit quality.

Our method has been applied to the Gravity Recovery and Climate Experiment (GRACE) and to the Jason-1 Ocean Surface Topography missions. The GRACE mission consists of two identical spacecraft flying in a near polar, near circular orbit with an altitude of approximately 500 km, in order to map the gravity field of the Earth. The spacecraft have a nominal separation of 220 km. Each satellite is equipped with a JPL BlackJack GPS receiver (dual-frequency, semi-codeless) [12]. Raw GRACE GPS measurements are available on the PODAAC website [13]. Precise orbits for the GRACE satellites are also available at PODAAC. The JPL orbit 3-D accuracy is around 3 cm RMS [12].

The Jason-1 mission is the follow-on to the French-American TOPEX/Poseidon mission. It has been designed to provide a reference map of the height of the oceans every ten days with a precision of only a few centimeters. To achieve this goal, Jason-1 is equipped with the best measurement systems currently available (a NASA/JPL Blackjack GPS receiver, a CNES DORIS (Doppler Orbitography and Radiopositioning Integrated by Satellite) receiver, a laser retroreflecting array), a high precision altimeter and a three frequency nadir looking radiometer. In addition to carrying precise sensors, Jason-1 flies at a high altitude of around 1330 km where drag is not a major perturbation, and its thrust-free reaction wheel based attitude control minimizes orbital perturbations. CNES computes the operational precise orbits of Jason-1 for the scientific altimetry community. The operational CNES precise orbit is a 3-technique solution mixing DORIS, GPS and SLR measurements; its accuracy is around 1 cm on

the radial component [14]. CNES also coordinates the efforts of scientists involved in the calibration and validation activities aimed at guarantying orbit precision. As part of this effort, NASA/JPL and the University of Colorado investigated the possibility of fixing ambiguities on double difference GPS data [15], but results were not as convincing as expected.

WIDELANE AMBIGUITY FIXING

JPL BlackJack GPS receivers on GRACE and on Jason-1 behave exactly like other ground based semi-codeless receivers. The GPS satellites' fractional widelane delays identified for semi-codeless ground-based receivers work with these spaceborne receivers as can be seen on Figure 13: the upper plot shows Jason-1 raw widelane measurements before correction, the lower plot shows these same data corrected for fractional widelane delays. Widelane residuals clearly gather around integers and widelane ambiguity blocking is straightforward.

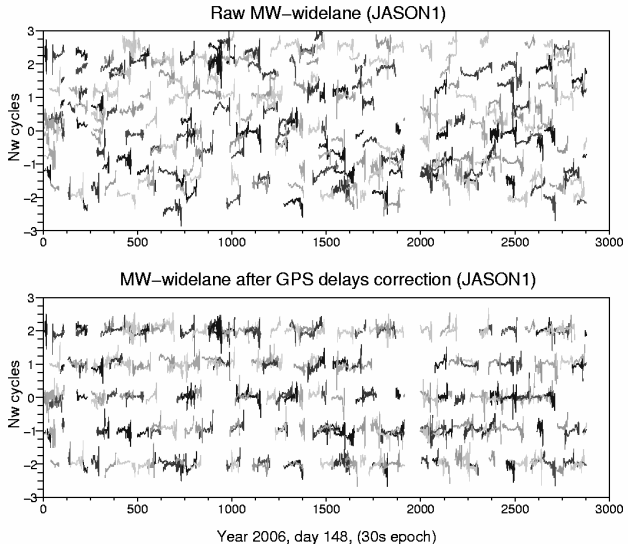

Fig. 13. Widelane residuals on Jason1 before and after delay correction

N_1 FIXING

The technique for N_1 ambiguity fixing on spaceborne data is derived from the strategy used for ground-based receivers. First, ionosphere-free phase residuals $R_c = \left(Q_c - D_w + h^j\right)/\lambda_c$ are computed using the most precise orbits available for the LEO satellite, IGS precise orbits for the GPS satellites [9], and GPS integer clocks consistent with the fractional widelane delays used during widelane ambiguity fixing (computed using a global network solution).

From equation (6) these residuals are equal to $R_c = -N_1 + h^j / \lambda_c$. By computing single differences of these residuals for all couples of GPS satellites it is possible to eliminate the receiver clock to reveal the integer nature of N_1 . Figure 14 shows the histogram of the fractional part of these single differences for all GRACE measurements from day 115 (as all possible single differences were computed, each difference appears twice with opposite signs leading to a symmetrical histogram). The statistic is broadly peaked around 0, due to errors in the GRACE orbit (a 3 cm error can lead to more than half a cycle error on some single differences).

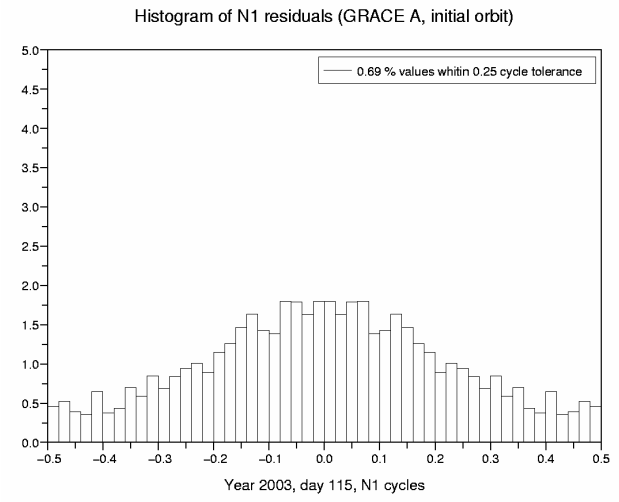

Fig. 14. Statistics of single-difference N_1 residuals (Grace A initial orbit)

In order to fix ambiguities, the orbit precision must be improved. However, the radial component of the orbit is always determined with a much better precision than the other components (in a dynamical orbit determination, the radial direction is the parameter which is the most observable because of its relation to the orbital period through Kepler's third law). The radial component thus does not need to be corrected. Applying small corrections on the along-track and cross-track components is therefore sufficient to improve the integer characteristics of N_1 ambiguities. These corrections are applied as time-correlated offsets on each component.

In our solution, offsets are constant per 5 minute batch. For one day of data and one satellite we simultaneously adjust one integer ambiguity per pass (about 400 passes), two offsets per batch (288 batches) and stochastic clock at each epoch (2880 values for 30 s data).

The initialization phase is performed with a standard least squares filter, with floating ambiguities. A bootstrap method is applied to progressively fix ambiguities: ambiguities which have the lowest covariance and are close to an

integer are fixed iteratively. More than 95% of all ambiguities are fixed in this process. The values of the corresponding orbit corrections are shown on Figure 15 for the GRACE satellites. The along-track correction is dominated by a contribution at the orbital period probably due to surface forces. The behavior of the cross-track correction is more chaotic.

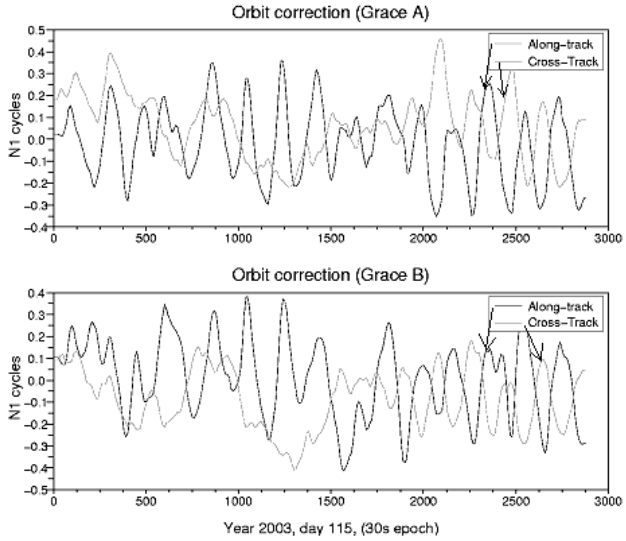

Fig. 15. Along-track and cross-track corrections to the GRACE JPL orbits needed for integer ambiguity fixing

PRECISE ORBIT DETERMINATION

Once ambiguities have been fixed unambiguous phase measurements can be used as very precise pseudo-range like data in a standard precise orbit determination solution. This way, resulting orbits are actual dynamical orbits, not empirically corrected orbits. However, thanks to the high observability provided by the very precise unambiguous phase data, it is possible to relax the dynamics to closely follow measurements. In our tests, absolute precise orbit determination is done with the CNES ZOOM software. This multi-purpose orbit determination filter is used routinely for the operational precise orbit determination of the Jason and Envisat altimetry missions [15]. This software implements some of the most sophisticated dynamical and measurement models available today. Table 3 lists the models used for Jason orbit determination.

Table 3. Jason-1 POD settings

Settings	Comment
Static gravity field	EIGEN GL04S (http://icgem.gfz-potsdam.de/ICGEM/ICGEM.html)
Time varying gravity field	Drift, annual, semiannual 50x50 from EIGEN-GL04S-ANNUAL

	(http://bgi.cnes.fr:8110/geoid-variations/static/EIGEN_GL04S_ANNUAL)
Atmospheric gravity	NCEP-derived 20x20 field at 6 hr interval (http://gemini.gsfc.nasa.gov/agra/)
3rd body gravity	Moon, Sun, planets
Solid Earth tides	IERS 2003 standards (http://www.iers.org/documents/publications/tn/tn32/tn32.pdf)
Ocean tides	FES 2004, all principal constituents, with admittance
Polar motion	IERS Bulletin A (http://maia.usno.navy.mil/)
Solar radiation pressure	Box and wings model with 0.97 constant scale factor (http://www.aviso.oceanobs.com/en/calval/orbit/index.html)
Earth albedo	Knocke-Ries albedo and infrared model
Atmospheric drag	DTM94 density model, 3 adjusted drag coefficients per orbit
Empirical forces	tangent and cross-track once per revolution, constant per 6 hours
Measurements	ionosphere-free combination for pseudo-range and phase, 30 second sampling one integer ambiguity per pass
GPS orbits and clocks	JPL IGS orbits, our own integer clocks
GPS antenna maps	JPL GPS and Jason-1 phase maps
State vector	6 orbital components 3 drag coefficients per orbit Along- and cross-track empirical accelerations every 6 hours stochastic clocks at each epoch

In the case of GRACE the dynamical settings are slightly different, with a drag coefficient adjusted every 2000 seconds on each spacecraft. The same settings are used for both GRACE-A and GRACE-B.

Figure 16 shows the statistics of GRACE-A and Jason-1 single difference N_1 residuals on the final orbits. When compared with Figure 14 which was obtained with the initial orbits, the integer nature of the residuals is clearly improved. Results obtained for Jason are slightly better.

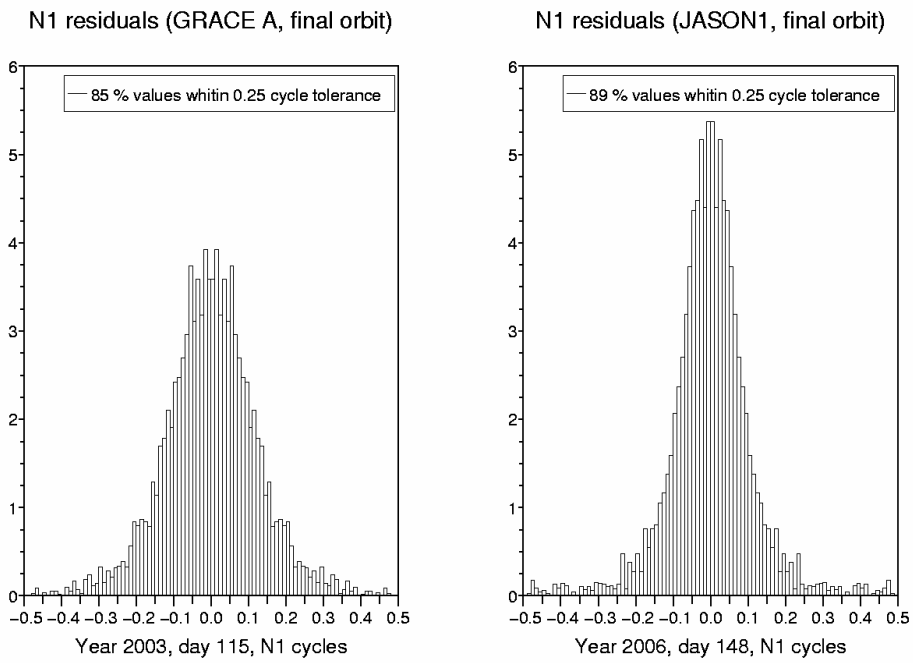

Fig. 16. Statistics of single-difference N_1 residuals (Grace A and Jason-1 final orbits)

VALIDATION OF AMBIGUITY FIXED GRACE ORBITS

The GRACE-A to GRACE-B inter-satellite K-Band range is a direct measurement of the relative satellite positions which can be used as a reference to evaluate the absolute orbits' precision. Figure 17 shows the difference between the distance computed by differencing the two absolute orbits and the inter-satellite range. The Root Mean Square of the difference is 2 mm, close to the best reported results [12]. This means that we can achieve as good a relative performance by differencing two absolute zero-difference orbits as with the state of the art relative orbit determination process.

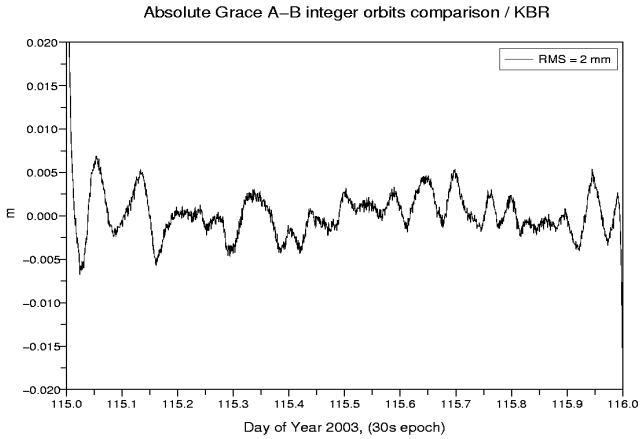

Fig. 17. Absolute baseline estimation vs. KBR

Because of the short distance between the satellites, and the fact that the GPS integer clocks are the same in the two absolute orbit determinations, one should not conclude that the absolute orbits are of millimeter accuracy, only the difference is. However, this proves that the zero-difference ambiguity estimation is correct for both satellites.

VALIDATION OF AMBIGUITY FIXED JASON ORBITS

An extensive study of this ambiguity fixed orbit solution has been conducted on Jason-1. In order to perform a significant evaluation, 148 days were processed (from 3/3/2006 to 7/29/2006), about fifteen Jason 10-day cycles (cycles 153 to 167), which is more than one complete rotation of the orbital plane relative to the sun.

The orbit solutions were computed on daily arcs using the method described above. Figure 18 presents the N_1 ambiguity fixing success rate during the entire test. The average fixing success rate is around 98% and most of the time above 95%.

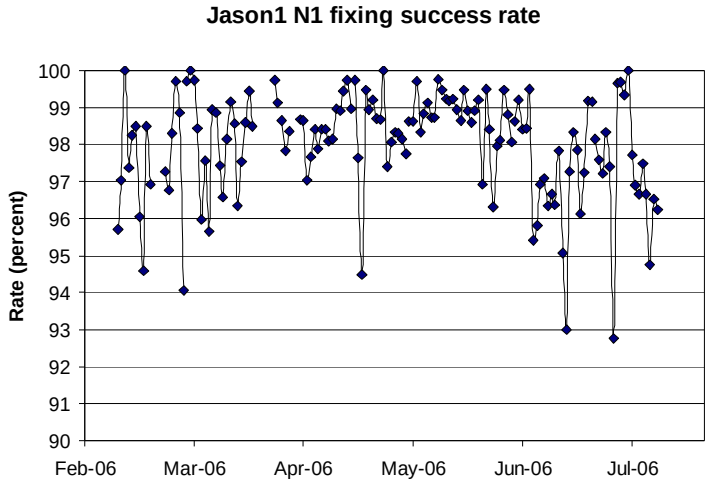

Fig. 18. Jason-1 ambiguity fixing statistics

For comparison purposes, orbits where ambiguities are not fixed but estimated as floating parameters in the state vector (all other settings being the same) are also computed. These orbits will be called 'floating' orbits as opposed to the fixed ambiguity orbits which will be referred to as 'integer' orbits.

First it should be stressed that measurement residuals are an indicator of the solution's internal quality which does not directly translate into orbit precision. This is clearly visible on Figure 19 which shows the daily RMS of the phase measurement residuals for both sets of orbits.

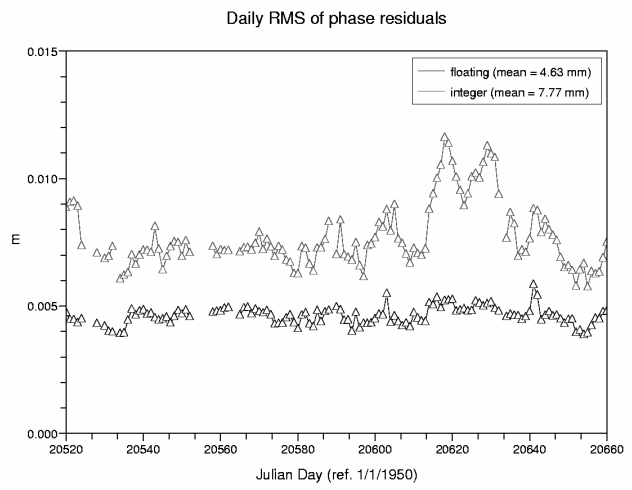

Fig. 19. Daily RMS values, floating and integer orbits

Residuals of floating orbits (lower curve) are significantly smaller than residuals of integer orbits (upper curve). This is explained by the larger number of adjusted parameters in the state vector for floating orbits. The fact that measurement residuals are lower than the expected orbit precision indicates that part of the orbit error is absorbed in the floating ambiguities. This clearly demonstrates that the floating solution offers lower observability. Integer orbits phase residuals are more in line with the actual orbit precision. The increase in residuals toward the end of the test appears as the same time as the reduced N_1 fixing success rate, but no explanation has yet been found for these effects (this will be investigated in the future).

The strength of the Jason-1 mission comes from the fact that it offers external measurements to evaluate orbit precision. Altimeter measurements are not used in the orbit determination process, so they can be used to evaluate orbit quality. An altimeter crossover measurement is a difference between two altitude measurements at a point where the ascending and descending ground tracks intersect. Common errors cancel at crossover points. The key contributors to crossover residuals are orbit error and ocean variability. Variability dominates the statistics, so crossover residuals are best used in a relative mode to compare orbit solutions. The analysis of crossover residuals is thus routinely used as an independent technique to inter-compare the radial accuracy of altimetry missions. Crossover residuals are computed on a 10-days cycle basis.

Figure 20 shows the difference between crossover residuals RMS computed with multiple orbits and integer orbits for each of the cycles in the test. Stars correspond to the floating orbits, circles to the operational GDR-C orbits [16] and triangles to the JPL series 07a orbits [17]. A positive difference indicates that the residuals are higher for the

standard orbit than for the integer orbit. The majority of the differences are positive, indicating a small but significant improvement in radial accuracy with integer orbits.

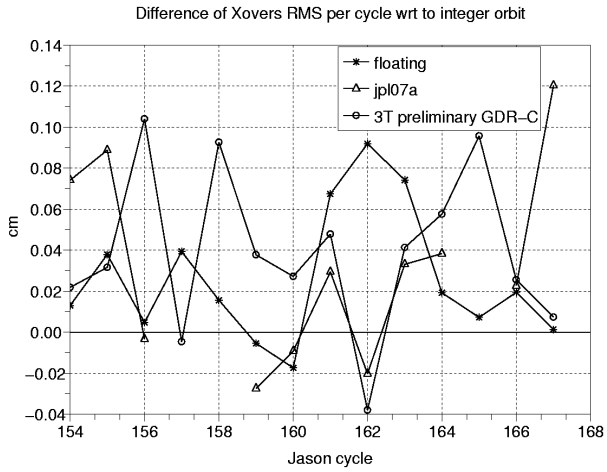

Fig. 20. Difference in altimeter cross-over residuals RMS between standard orbits and integer orbits

Satellite Laser Ranging (SLR) is another independent tracking technique [18] available on Jason-1. SLR residuals thus provide an indication of orbit quality. SLR residuals can be computed on a daily basis for a core network of laser stations for all orbits in order to intercompare them. CNES operational precise orbits are excluded from this test because SLR measurements are used in the orbit computation.

Figure 21 shows the difference between the daily RMS of SLR residuals computed with standard orbits and integer orbits. Stars correspond to 'floating' orbits, triangles to the JPL series 07a orbits. A positive difference indicates that the residuals are higher for the standard orbit than for the integer orbit. The majority of daily differences is positive, showing a mean improvement of around 1.5 mm in favor of the integer orbit, which is a significant result given the fact that the residuals themselves are around one centimeter.

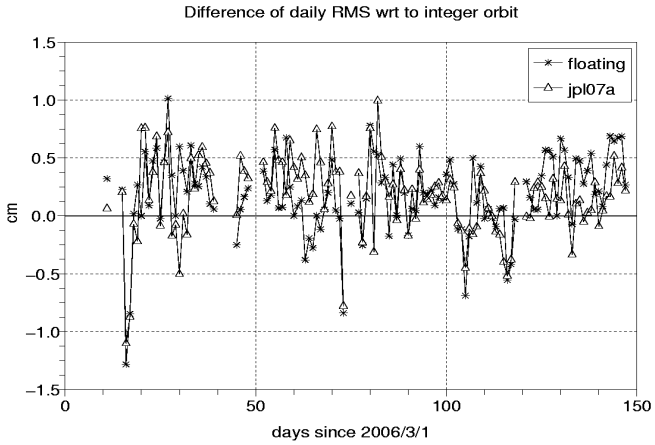

Fig. 21. Difference in SLR residuals RMS between standard and integer orbits

Figure 22 shows another characteristic of SLR residuals on integer orbits. It plots the SLR residuals as a function of elevation angle over the station. At high elevations SLR residuals measure the radial orbit error. At lower elevations they also measure a contribution from along-track and cross-track orbit error. Integer orbits clearly outperform standard orbits at all elevations.

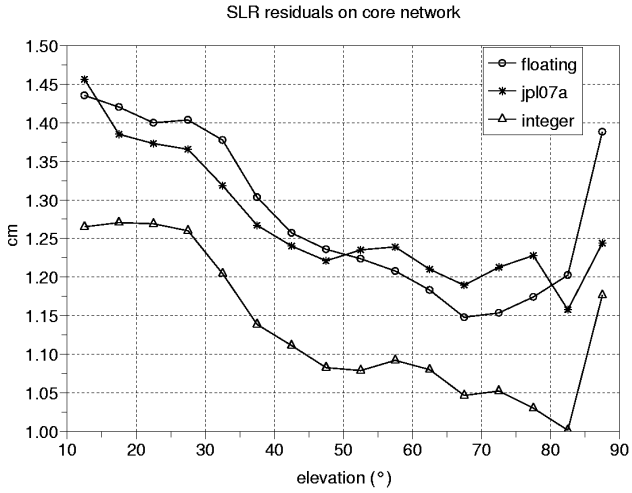

Fig. 22. Site dependant SLR residuals comparison

CONCLUSIONS

In this paper, we have presented an efficient method to fix widelane ambiguities on undifferenced GPS measurements, based on the simple assumption of the stability of delays at the GPS satellite level. This can be applied independently on each receiver. The use of the same satellite delays for all the receivers ensures that the

estimated unambiguous widelanes are coherent among receivers. Then, the fixing of undifferenced N_1 ambiguities on a network of stations, leads to improved 'integer' GPS clocks.

These widelane delays and improved clocks, associated to the GPS orbits, form a 'compact' representation of the whole constellation, which allows an easy fixing of ambiguities on the two frequencies for any receiver external to the initial network. Tests of positioning with both geodetic and moving receivers conducted at CNES using this method lead to an actual positioning precision at the centimeter level.

This approach can be used in post-processing or in real-time with similar performance.

The application to low Earth orbiting satellites appears to improve orbit precision. The relative position obtained by differencing absolute orbits for the two GRACE satellites agrees with the very precise inter-satellite K-band range measurements to within 2 millimeters RMS. On Jason-1, independent orbit quality checks using Satellite Laser Ranging measurements and altimeter crossover residuals show that the ambiguity fixed orbits are slightly but unmistakably more precise than state of the art solutions.

ACKNOWLEDGMENTS

The authors wish to thank M. Boschetti, J. Bijac, P. Van-Troostenberghe and J.L. Issler for their helpful comments and participation. They also wish to thank NASA for providing them with GRACE GPS data and precise orbits for GRACE and Jason-1. The authors acknowledge the contribution of the International GNSS Service and of the International Laser Ranging Service to their research effort.

REFERENCES

1. Kim D. and Langley R. B., *GPS Ambiguity Resolution and Validation: Methodologies, Trends and Issues*, 7th GNSS Workshop - International Symposium on GPS/GNSS, Seoul, Korea, Nov. 30-Dec. 2, 2000
2. Delporte J., Mercier F., Laurichesse D. and Galy O., *Fixing integer ambiguities for GPS carrier phase time transfer*, TimeNav May 2007, ENC-GNSS 07, Geneva
3. Gabor M. J., *GPS Carrier Phase Ambiguity, Resolution Using Satellite-Satellite Single Differences*, ION GPS 1999
4. Wang M. and Gao Y., *GPS Un-Differenced Ambiguity Resolution and Validation*, Proceedings of the ION GNSS-06 September 26-29, 2006, Fort Worth, Texas
5. Leandro R. F. and Santos M. C., *Wide Area Based Precise Point Positioning*, Proceedings of the ION GNSS-06, September 26-29, 2006, Fort Worth, Texas

6. Collins P., *Isolating and estimating undifferenced GPS integer ambiguities*, Proceedings of the ION NTM 2008, January 2008, San Diego, California
7. Dach R., Schildknecht T., Hugentobler U., Bernier L. and Dudle G., *Continuous Geodetic Time-Transfer Analysis Methods*, IEEE Transactions, Vol. 53, No 7,July 2006
8. Mercier F. and Laurichesse D., *Receiver/Payload hardware biases stability requirements for undifferenced Widelane ambiguity blocking*, Scientifics and fundamental aspects of the Galileo program Colloquium, Fall 2007, Toulouse, France
9. Dow J. M., Neilan R. E. and Gendt G., *The International GPS Service (IGS): Celebrating the 10th Anniversary and Looking to the Next Decade*, Adv. Space Res. 36 vol. 36, no. 3, pp. 320-326, 2005. doi:10.1016/j.asr.2005.05.125
10. Wübbena G., Schmitz M. and Bagge A., *PPP-RTK: Precise Point Positioning Using State-Space Representation in RTK Networks*, ION GNSS-05, September 13-16, 2005, Long Beach, California.
11. Laurichesse D., Mercier F., Berthias J-P., CNES and Bijac J., ATOS Origin, France *Real Time Zero-difference Ambiguities Blocking and Absolute RTK*, Proceedings of the ION NTM 2008, January 28-30, 2008, San Diego, California
12. Kroes R., *GRACE: Precise Relative Positioning of Formation Flying Spacecraft using GPS*, Publications on Geodesy 61 Delft, March 2006, ISBN-10: 90 6132 296 0
13. *PODAAC ftp site* : ftp://podaac.jpl.nasa.gov/pub/grace/
14. Berthias J-P. and Ries J., *POD & Geoid section*, 2007 OSTST Executive summary, Hobart, 2007
15. Yoon Y. T., *JASON: Resolving Carrier Phase Ambiguities for a Low Earth Orbit Spacecraft*, 2004 Ph.D. Thesis, University of Colorado
16. Cerri L., *GDRC standards for Jason-1*, DORIS Analysis Working Group meeting (AWG) of the International DORIS Service, Paris, March 13-14, 2008
17. Haines, B., private communication
18. Pearlman, M.R., Degnan, J.J., and Bosworth, J.M., *The International Laser Ranging Service*, Advances in Space Research, Vol. 30, No. 2, pp. 135-143, July 2002, DOI:10.1016/S0273-1177(02)00277-6